Applied Catalysis B: Environmental 179 (2015) 305–312

Contents lists available at ScienceDirect

Applied Catalysis B: Environmental

journal homepage: www.elsevier.com/locate/apcatb

Study of the phenol photocatalytic degradation over TiO_2 modified by sulfation, fluorination, and platinum nanoparticles photodeposition

J.J. Murcia [a,b,*], M.C. Hidalgo [b], J.A. Navío [b], J. Araña [c], J.M. Doña-Rodríguez [c]

[a] Grupo de Catálisis, Escuela de Ciencias Químicas, Universidad Pedagógica y Tecnológica de Colombia UPTC, Avenida Central del Norte, Tunja, Boyacá, Colombia

[b] Instituto de Ciencia de Materiales de Sevilla (ICMS), Consejo Superior de Investigaciones Científicas CSIC – Universidad de Sevilla, Américo Vespucio 49, 41092 Sevilla, Spain

[c] CIDIA (Departamento de Química), Universidad de las Palmas de Gran Canaria, Edificio del Parque Científico Tecnológico, Campus Universitario de Tafira, 35017 Las Palmas de Gran Canaria, Spain

ARTICLE INFO

Article history:
Received 16 December 2014
Received in revised form 15 May 2015
Accepted 20 May 2015
Available online 22 May 2015

Keywords:
TiO_2
Sulfation
Fluorination
Pt photodeposition
Phenol photodegradation

ABSTRACT

In this work, titanium dioxide has been modified by sulfation, fluorination and simultaneous Pt nanoparticles deposition; the influence of these treatments on the photocatalytic activity of this oxide has been studied. A complete characterization study was carried out and it was observed that sulfation, fluorination and metallization were important factors influencing the TiO_2 properties. The photocatalytic activity of the materials prepared was evaluated in the phenol degradation and it was found that TiO_2 fluorination significantly increased the phenol photodegradation rate, compared with bare TiO_2, sulfated TiO_2 or the commercial TiO_2 Degussa P25. It was also found that Pt photodeposition on sulphated TiO_2 notably increased the photocatalytic activity of this oxide, while Pt on fluorinated TiO_2 did not modify significantly the phenol photodegradation rate.

1. Introduction

Titanium dioxide (TiO_2) heterogeneous photocatalysis has been studied in the decomposition of a wide range of undesirable chemical contaminants and it appears to be a feasible process for water and air pollution control by using solar or artificial light illumination.

TiO_2 properties, such as phase composition and structure, surface hydroxyl groups, particle size, and surface defects play a very important role in the activity of this oxide in photocatalytic reactions. In different studies, some of these parameters have been modified in order to enhance the photocatalytic performance of the TiO_2 [1–8].

It is generally accepted that one major draw-back of TiO_2 as a photocatalyst is the high recombination rate of the electron–hole pair photogenerated, which reduces the photoefficiency of the photocatalytic process.

The sulfation of TiO_2 surface has been reported as an effective method for improving the photoefficiency of this oxide [9–11]. Sulfation pre-treatment leads to a stabilization of the TiO_2 anatase crystalline phase and surface area against sintering during the calcination process. A dehydroxylation process of the excess of adsorbed protons takes place during calcination, leading to the creation of surface oxygen vacancies and promoting the separation of photogenerated charges, thus, improving the TiO_2 photocatalytic efficiency.

As another method for improving the photocatalytic activity of TiO_2, different authors have studied the surface fluorination as a new approach of TiO_2 surface modification [12–18]. Firstly, it has been reported that the surface fluorination of TiO_2 leads to the formation of surface ≡Ti–F groups, these species have a strong electron-withdrawing ability leading to the reduction of the recombination of the photogenerated electrons and holes [14,15,19]. On the other hand, it has also found that surface fluorination of TiO_2 enhances the generation of mobile (unbound) $OH^{\bullet}$ radicals that are stronger oxidants than the surface adsorbed $OH^{\bullet}$ radicals [13,17,19,20]. These are the main effects explaining the enhanced photocatalytic activity of fluorinated TiO_2.

Additionally, noble metal deposition has also been a common strategy used to improve the photoefficiency of TiO_2. In this case, the noble metal deposits (usually Au, Pt, Ag, and/or Pd) on TiO_2

* Corresponding author at: Instituto de Ciencia de Materiales de Sevilla (ICMS), Américo Vespucio No. 49, 41092 Sevilla, Spain. Tel.: +57 3045229025; fax: +57 0387425268.
E-mail address: jjuliejoseane@hotmail.com (J.J. Murcia).

http://dx.doi.org/10.1016/j.apcatb.2015.05.040
0926-3373/

surface act as receptors of the electrons photogenerated in the illuminated TiO_2, thus, reducing the recombination rate and therefore improving the photocatalytic activity of this oxide [2,5,6,8,10,21].

This manuscript describes the synthesis of a series of TiO_2 powders modified by sulfation, fluorination and platinum addition. The main objective of this work has been to study the combination effect of platinization on sol–gel prepared TiO_2 previously sulfated or fluorinated. The photocatalytic activity of the TiO_2 powders prepared was studied in phenol photodegradation used as test reaction. The properties of bare and modified TiO_2 are described in detail and a comparative study of the photocatalytic activity of the TiO_2 powders obtained is also presented.

2. Experimental

TiO_2 used as starting material (bare TiO_2) was prepared by hydrolysis of titanium tetraisopropoxide (Aldrich, 97%) in isopropanol solution (1.6 M) by the slow addition of distilled water (volume ratio isopropanol/water 1:1). The TiO_2 powder was recovered by filtration and dried at 110 °C for 24 h and then this was calcined at 650 °C for 2 h.

Also non calcined TiO_2 powder was modified by sulfation or fluorination treatments, thus, sulfated TiO_2 (S–TiO_2) sample was obtained by immersion of the uncalcined TiO_2 powder in a 1 M sulfuric acid solution under continuous stirring for 1 h, followed by filtration, drying, and calcination at 650 °C for 2 h.

Fluorinated TiO_2 (F–TiO_2) was prepared by adding 10 mM NaF to an aqueous suspension of uncalcined TiO_2. The pH was then adjusted to 3 using a solution of HCl 1 M to maximize the fluoride adsorption. This suspension was stirred for 1 h in the dark. Precipitate was recovering by filtration, dried, and calcined at 650 °C for 2 h.

Photodeposition of platinum was performed over the calcined TiO_2 powders (bare TiO_2, S–TiO_2, or F–TiO_2) using hexachloroplatinic acid (H_2PtCl_6, Aldrich 99.9%) as metal precursor. Under an inert atmosphere (N_2), a suspension of the corresponding TiO_2 sample in distilled water containing isopropanol (Merck 99.8%) which acts as sacrificial donor was prepared. Then, the appropriate amount of H_2PtCl_6 to obtain a nominal platinum loading of 0.5% weight total to TiO_2 was added. Final pH of the suspensions was 3. Photodeposition of platinum was then performed by illuminating the suspension for 120 min with an Osram Ultra-Vitalux lamp (300 W) which possesses a sun-like radiation spectrum with a main emission line in the UVA range at 365 nm. Light intensity on the suspensions was 60 W/m^2 determined by a PMA 2200 UVA photometer (Solar Light Co.). After photodeposition, the powders were recovered by filtration and dried at 110 °C overnight.

Commercial TiO_2 Degussa P25 used as reference material was employed as received.

All the materials were widely characterized using different techniques. Crystalline phase composition and degree of crystallinity of the samples were estimated by X-ray diffraction (XRD). XRD patterns were obtained on a Siemens D-501 diffractometer with Ni filter and graphite monochromator using Cu Kα radiation. Anatase crystallite sizes were calculated from the line broadening of the main anatase X-ray diffraction peak (1 0 1) by using the Scherrer equation. Peaks were fitted by using a Voigt function.

Specific surface area (S_{BET}) measurements were carried out using low-temperature nitrogen adsorption in a Micromeritics ASAP 2010 instrument. Degasification of the samples was performed at 150 °C.

Chemical composition and total platinum content in the samples were determined by X-ray fluorescence spectrometry (XRF) in a Panalytical Axios sequential spectrophotometer equipped with a rhodium tube as the source of radiation. XRF measurements were performed onto pressed pellets (sample included in 10 wt.% of wax).

Light absorption properties of the samples were studied by UV–vis spectroscopy. The UV–vis DRS spectra were recorded on a Varian spectrometer model Cary 100 equipped with an integrating sphere and using $BaSO_4$ as reference. Band-gaps values were calculated from the corresponding Kubelka–Munk functions, F($R\infty$), which are proportional to the absorption of radiation by plotting $(F(R\infty) \times h\nu)^{1/2}$ against $h\nu$.

Platinum particle sizes were evaluated by Transmission Electronic microscopy TEM, using a microscope Philips CM 200. For these analyzes, samples were dispersed in ethanol using an ultrasonicator and dropped on a carbon grid.

X-ray photoelectron spectroscopy (XPS) studies were carried out on a Leybold–Heraeus LHS-10 spectrometer, working with constant pass energy of 50 eV. The spectrometer main chamber, working at a pressure $<2 \times 10^{-9}$ Torr, is equipped with an EA-200 MCD hemispherical electron analyzer with a dual X-ray source working with Al Kα ($h\upsilon$ = 1486.6 eV) at 120 Wand 30 mA. C 1s signal (284.6 eV) was used as internal energy reference in all the experiments. Samples were outgassed in the prechamber of the instrument at 150 °C up to a pressure $< 2 \times 10^{-8}$ Torr to remove chemisorbed water.

Difusse reflectance infrared Fourier transform spectroscopy (DRIFTS) spectra were recorded on a Thermo Scientific-Nicolet iS10 spectrophotometer. Intervals of 4000–1000 cm^{-1}, a resolution of 2 cm^{-1}, and a forward and reverse moving mirrors speed of 10 and 6.2 kHz, respectively, were used.

Phenol photocatalytic degradation reactions were carried out using a discontinuous batch of 400 mL pyrex reactor enveloped by an aluminum foil, filled with an aqueous suspension (250 mL) containing 50 ppm of phenol (0.53 mM) and photocatalyst (1 g/L). This system was illuminated through a UV-transparent Plexiglas® top window (threshold absorption at 250 nm) by anOsram Ultra-Vitalux lamp (300 W) with sun-like radiation spectrum and a main line in the UVA range at 365 nm, the intensity of the light on photoreactor was 140 W/m^2. In order to favor the adsorption–desorption equilibrium, prior to irradiation the suspension was magnetically stirred for 10 min in dark. Magnetic stirring and a constant oxygen flow of 35 L/h as an oxidant were used to produce a homogeneous suspension of the photocatalyst in the solution. All photocatalytic tests started at pH ca. 6 and the total reaction time was 120 min. During the phenol photoreaction, samples were collected at different times and measured by HPLC, using an Agilent Technologies 1200 chromatograph, which was equipped with UV–vis detector and an Elipse XDB-C18 column (5 μm, 4.6 mm × 150 mm). The HPLC analysis was carried out using water/methanol (65:35) as mobile phase, a flow rate of 0.8 mL/min and 40 °C.

Photolysis test of phenol under UV light and in absence of catalyst were carried out. Under the experimental conditions used in this work, phenol photolysis was not observed.

Total mineralization of phenol with the illumination time was followed by measuring the total organic content (TOC) in a Shimadzu 5000 TOC analyzer.

3. Results and discussion

3.1. Photocatalysts characterization

3.1.1. X-ray diffraction

XRD was used to analyze the effects of fluorination, sulfation, and platinization on the crystallite structure and phase composition of TiO_2 prepared by sol–gel method. Fig. 1A and B shows the XRD patterns of the bare and modified TiO_2.

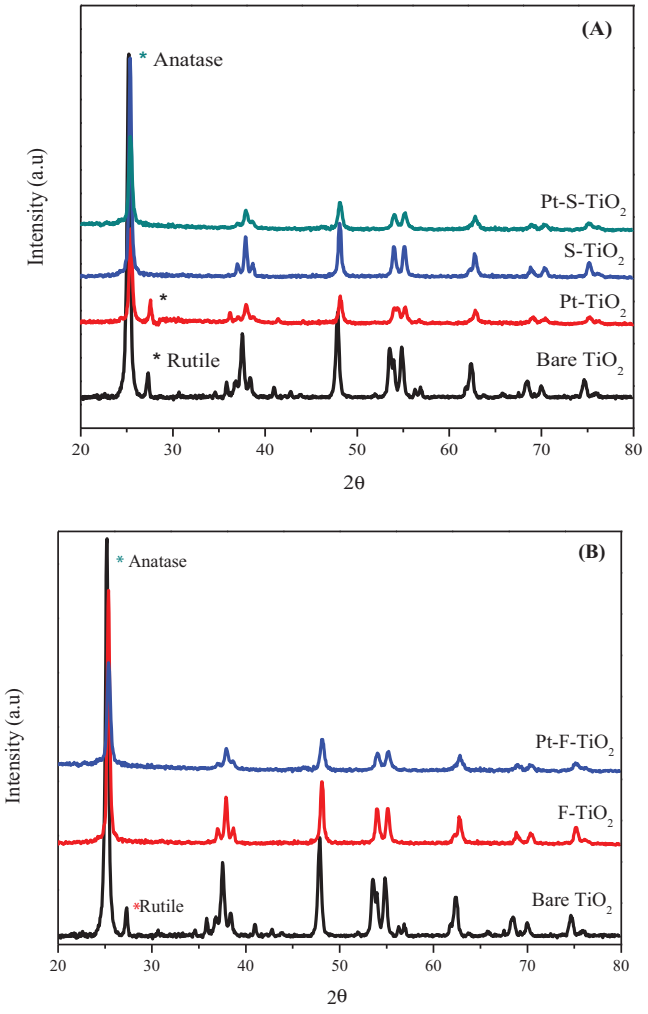

Fig. 1. XRD patterns for TiO_2 modified by sulfation, fluorination and Pt photodeposition. (A) Sulfated samples and (B) fluorinated samples.

Bare TiO_2 and Pt–TiO_2 samples present anatase and rutile phases, identified by the main XRD peaks at 25.25° and 27.44° respectively, in a ratio about 90% anatase and 10% rutile. In contrast, in the TiO_2 modified by sulfation or fluorination, the only crystalline phase present was anatase, thus, indicating that these pre-treatments inhibited the formation of rutile phase of TiO_2 during the calcination process, as it has been reported by different authors [10,11,22,23]. On the other hand, photodeposition of platinum does not affect the phase composition in any case. In the spectra of metallized samples, no diffraction peaks for Pt were detected surely due to the low metal content and Pt particle size in these samples which is under the detection limit of the technique.

The anatase crystallite sizes calculated by the Scherrer equation from the (1 0 1) peak of the XRD pattern are listed in Table 1. Bare TiO_2 and Pt–TiO_2 present values of 17 and 18 nm respectively, which increases with the pre-treatment processes, more notably with fluorinarion reaching a size of 24 nm. These results are in agreement with reported studies [24,25] where it was seen that fluoride enhanced the crystallization of anatase phase and promoted the growth of crystallites. As it can also be observed in Table 1, the platinization of the samples did not modify crystallite sizes further.

3.1.2. BET surface areas

BET surface area values (S_{BET}) for all samples are also shown in Table 1. Bare TiO_2 with 11 m^2/g, presented the lowest specific surface area of all samples, as a consequence of the large degree of particles sintering during the calcination process. As seen in Table 1, sulfation and fluorination pre-treatments are beneficial for obtaining materials with larger surface areas, these ions protect anatase phase against rutilization and sintering, preserving the surface area during the calcination process. Highly crystalline material is obtained after calcination of S–TiO and F–TiO_2 samples at 650 °C, as it was also observed by DRX analyzes.

Platinization did not induce significant modifications in the S_{BET} of the analyzed materials and the observed slight decreases are probably due to pore blocking by metal deposits on the TiO_2 surface.

3.1.3. Microscopic analysis

Fig. 2 shows representative TEM images of bare (Fig. 2A), sulfated (Fig. 2B), and fluorinated (Fig. 2C) TiO_2 after platinum photodeposition. In all the samples, platinum particles can be seen as dark spherical spots placed on the larger anatase particles. On the sulfated TiO_2, platinum particles appear homogenously distributed all over the surface and with sizes around 4–5 nm. As it has been reported, sulfation of TiO_2 improves Pt photodeposition by producing a higher dispersion and smaller average deposit size of platinum [10]. On bare TiO_2 and fluorinated TiO_2 samples, metal deposits appear less homogenously distributed and with an average particle size larger than for the sulfated TiO_2, with metal particles sizes >5 nm. Thus, according to TEM studies, sulphated TiO_2 is the best support for platinum photodeposition.

3.1.4. X-ray fluorescence

The real platinum content in the metallized samples was measured by XRF and it was 0.29, 0.30, and 0.39% for Pt–TiO_2, Pt–S–TiO_2, and Pt–F–TiO_2 samples, respectively. These values are under the nominal metal content used to prepare these materials (0.5 wt.%), indicating an incomplete reduction of the metal precursor on TiO_2 surface during the photodeposition process. However, it was observed that the amount of deposited Pt was higher in the fluorinated sample.

XRF analysis revealed that a certain amount of S and Cl^- species remained on the solids after preparation. The sulfur content in sulfated materials was 0.66 and 0.16% for S–TiO_2 and Pt–S–TiO_2 samples, respectively. The Cl^- content in all the platinized samples was under 0.10%; this content comes from H_2PtCl_6 used as metal precursor. In the fluorinated samples, no F^- or Na content could be detected by XRF.

3.1.5. XPS analyzes

XPS measurements were performed and a summary of these results is reported in Table 1 and Fig. 3 shows XPS spectra of different regions obtained for selected samples, all the spectra were calibrated with the C 1s peak at 284.6 eV attributed to adventitious surface carbon. Spectra of Cl 2p and S 2p regions are not shown because due to the lower content of these elements in the analyzed samples the signal noise not permit to do an accurate appreciation of them.

The Ti 2p core peaks exhibit a main component at around 458.4 ± 0.1 eV (Ti $2p_{3/2}$) in all the samples; this is representative of the Ti^{4+} ions in TiO_2 lattice.

In the O 1s region, a peak located at 529.6 ± 0.2 eV can be observed for all the samples, it is assigned to oxygen atoms in the TiO_2 lattice. This peak is asymmetric with a shoulder located at higher binding energies; this peak is assigned to surface OH groups. The shoulder is more prominent in the F–TiO_2 sample, indicating a higher hydroxylation degree in this sample.

The estimation of O/Ti atomic ratios (Table 1) indicated an increase of surface OH group content after the fluorination. O/Ti values reached a maximum of 2.0 for F–TiO_2. This result highlights the creation of surface hydroxyls (OH) groups after fluorination of TiO_2. Similar results have been reported by Le et al. [15]; these authors

Table 1
Summary of the characterization results.

Catalyst	$D_{Anatase}$ (nm)	S_{BET} (m^2/g)	Binding energy (eV)		Band gap(eV)	O/Ti
			Ti $2p_{3/2}$	O 1s		
P25	22	51	458.5	529.8	3.23	1.87
Bare TiO_2	17	11	458.5	529.8	3.30	1.96
Pt–TiO_2	18	13	458.7	530.0	3.22	1.92
S–TiO_2	20	58	458.5	529.8	3.20	1.70
F–TiO_2	24	51	458.4	529.6	3.21	2.0
Pt–S–TiO_2	20	49	458.4	529.6	3.20	1.91
Pt–F–TiO_2	23	42	458.4	529.8	3.24	1.90

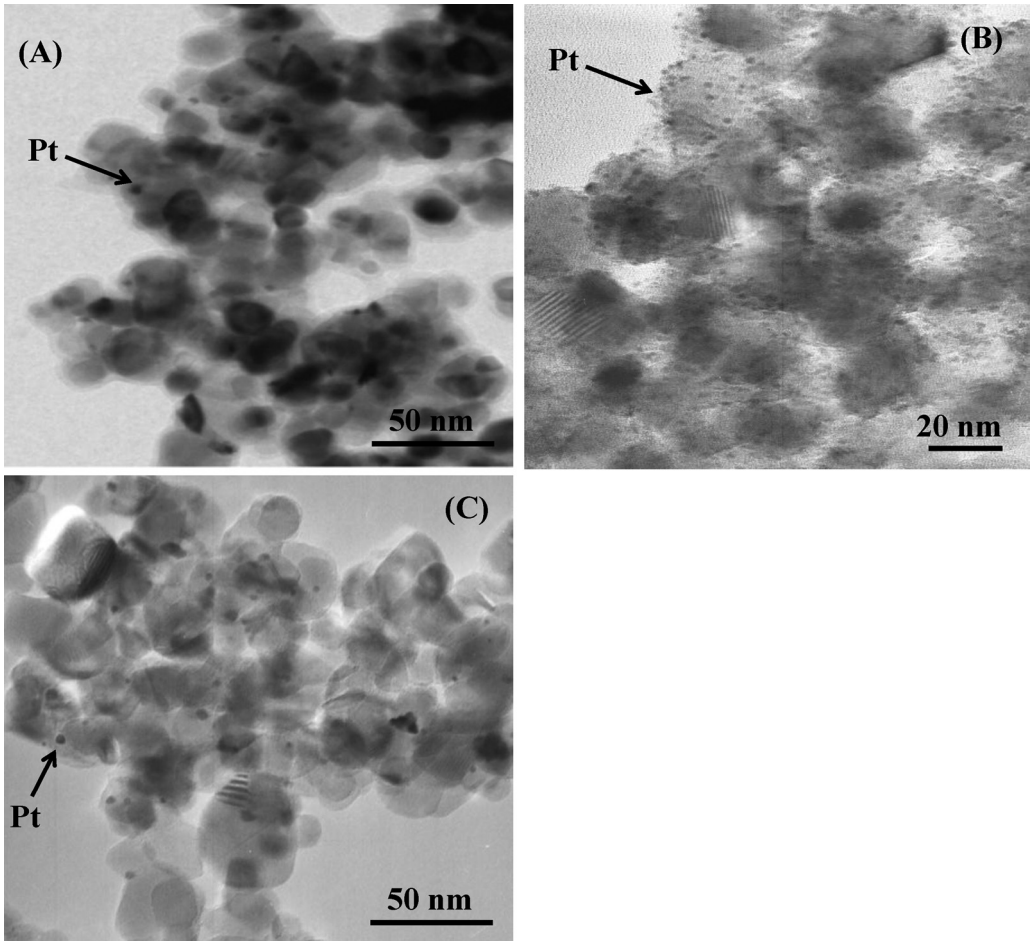

Fig. 2. TEM images of platinized TiO_2. (A) Pt–TiO_2, (B) Pt–S–TiO_2, and (C) Pt–F–TiO_2.

have also observed an increase of surface OH group content after the fluorination.

In metallized samples, the lowest hydroxylation degree is observed, this is due to the high number of Pt nanoparticles deposited on TiO_2 surface, as it can be observed in TEM images (Fig. 2).

By XPS also F 1s region was analyzed. In this region, it was observed a main peak located at the binding energy of 684 eV (Fig. 3), this peak is due to surface fluoride (≡Ti–F) formed by ligand exchange reaction between F^- and the surface hydroxyl group on TiO_2 surface [20,24], the atomic contents of F on the surface of fluorinated samples measured by XPS were 1.83 and 1.12% for F–TiO_2 and Pt–F–TiO_2 samples, respectively.

By XPS it was also detected a remaining content of Cl, S, F, and Na even after calcination process at 650 °C; thus, traces of Cl and S were detected in all the samples; the atomic content of these elements was below of 0.47 and 1.64%, respectively. Lower remaining contents of Na were also detected on the surface of the fluorinated samples (i.e., >2.0%). Fig. 3 shows the spectra of the F 1s and Na 1s regions for the fluorinated samples.

3.1.6. UV–vis diffuse reflectance spectra

The absorption spectra of all the samples are shown in Fig. 4. The typical absorption band edge of the TiO_2 semiconductor was observed at around of 400 nm for all the samples. As it can be seen, the UV–vis absorption of the fluorinated TiO_2 samples is slightly higher than that of the other samples whereas, the absorption edge region is almost unaffected by the surface fluorination, the absorption in the visible range could indicate the formation of surface defects (i.e., oxygen vacancies within the anatase structure). The occurrence of these oxygen vacancies takes place during calcination of the fluotinated or sulfated TiO_2 at 650 °C; however, F–TiO_2 absorbs at longer wavelengths with respect to S–TiO_2 it could be

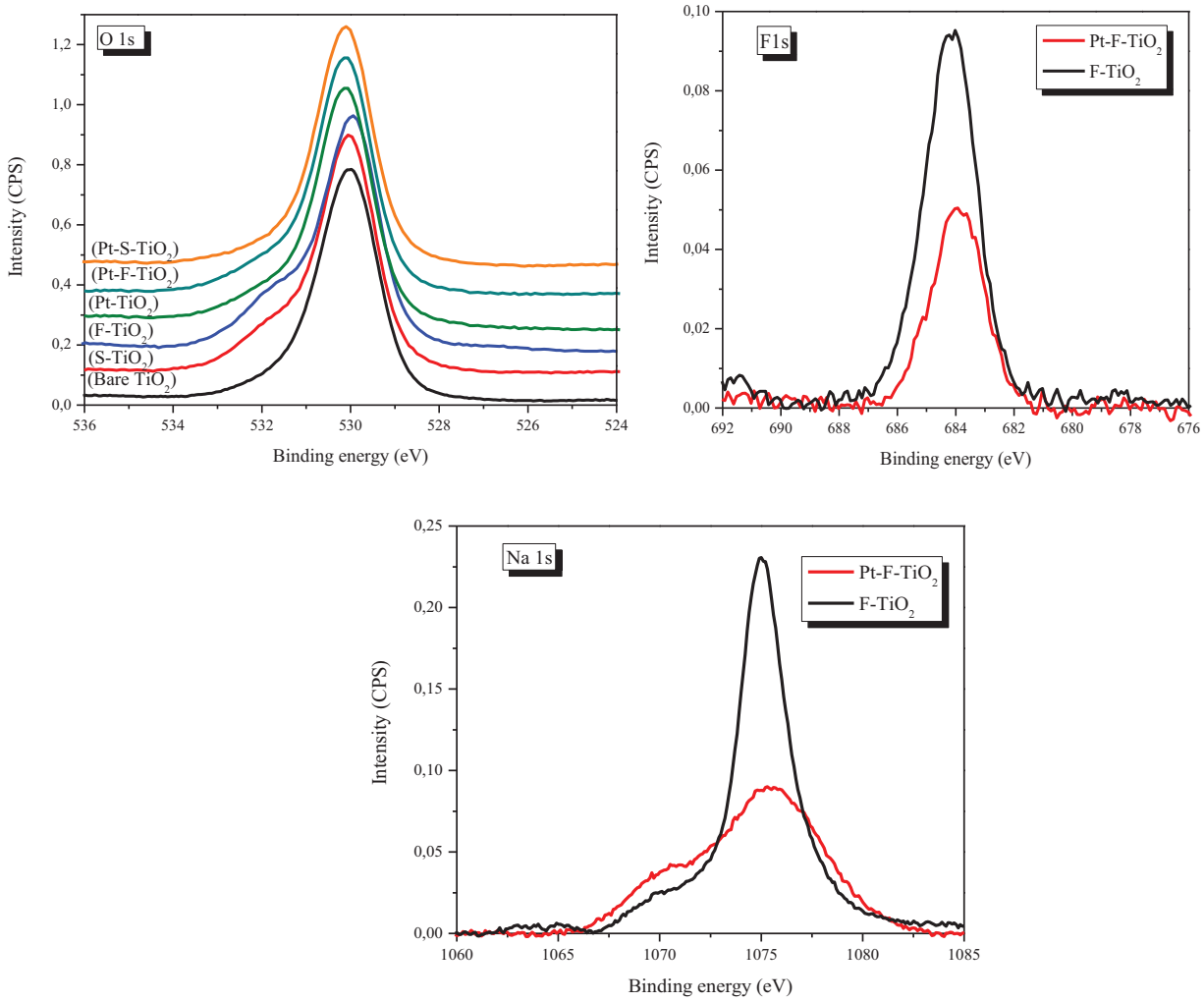

Fig. 3. XPS core level spectra of O 1s, F 1s, and Na 1s regions for selected samples.

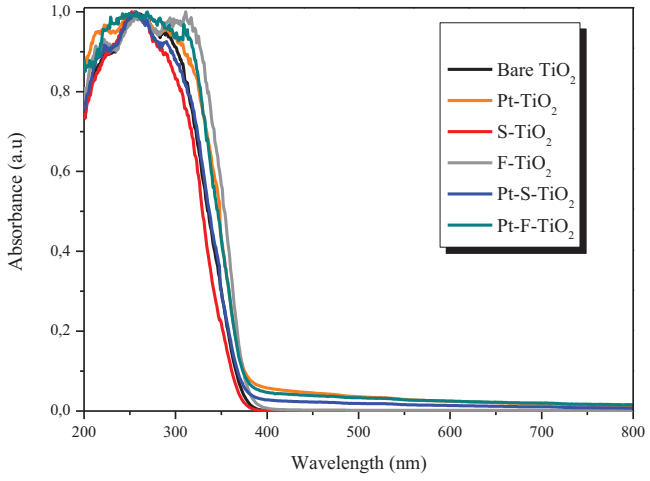

Fig. 4. UV–vis DRS spectra for analyzed samples.

due to the presence of a higher content of fluoride species (≡Ti–F) on F–TiO_2 surface, as it was observed by XPS (Fig. 3).

Platinization did not alter substancially the absorption properties of the samples, however, a slight increase of absorption throughout the visible range of the spectrum was observed due to the grey color of these materials.

From the UV–vis DRS spectra, band gaps energies were calculated and the obtained results are reported in Table 1, being 3.3 eV for the bare TiO_2. After sulfation, fluorination and/or platinization treatments a slight narrowing of the TiO_2 band gap was observed; the estimated band gap energies for these samples are between 3.17 and 3.23, these values are very close to that of anatase TiO_2 (3.20 eV).

3.1.7. FT-IR analyzes

The FT-IR spectra in the range between 4000 and 2400 cm^{-1} are presented in Fig. 5. A band located at 3698 cm^{-1} corresponding to isolated hydroxyl groups (Ti–OH(is)) was detected in all the samples.

Two clear bands located at 3393 cm^{-1} and at 3214 cm^{-1} were also detected. These absorptions have been assigned to terminal Ti–OH and adsorbed water Ti–OH_2 species, respectively [26–29].

The highest intensity of the band assigned to Ti–OH_2 is observed in the IR spectra obtained for the bare TiO_2, and S–TiO_2 samples; after fluoride addition, the intensity and width of this band considerably decrease, indicating a lower hydroxylation degree for F–TiO_2 sample. This is contradictory with the XPS results presented previously in Fig. 3; however, these differences could be explained taking into account that by FT-IR is evident that during the fluoride adsorption on TiO_2 surface (at pH 3 used for the synthesis of the F–TiO_2 sample), the ≡Ti–OH_2^+ species could be substituted by ≡Ti–F species, thus, reducing the intensity of the IR band character-

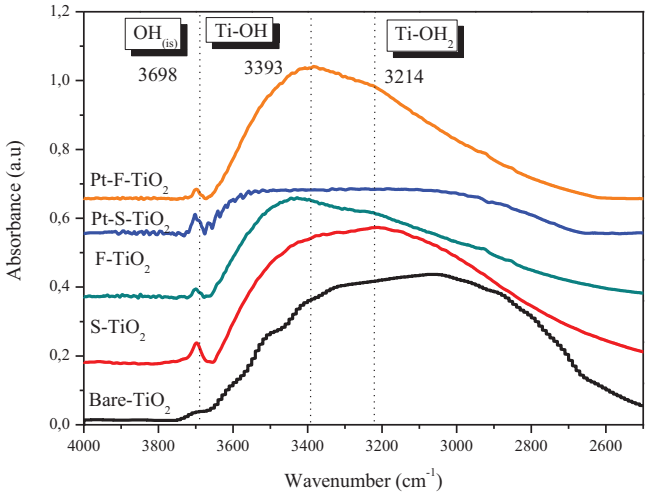

Fig. 5. IR spectra of the photocatalysts analyzed, hydroxyl groups region between 4000 and 2400 cm^{-1}.

istic of the hydration centers. In this process the following surface reactions take place:

$$\equiv Ti - OH^{+}{}_2 \leftrightarrow Ti - OH + H^{+} \quad (1)$$

$$\equiv Ti - OH \leftrightarrow TiO^{-} + H^{+} \quad (2)$$

$$\equiv TiO + H^{+} + F^{-} \leftrightarrow \equiv TiF + H_2O \quad (3)$$

The results obtained in the present work are consistent with the data reported by Vohra et al. [14], these authors also have found that the fluoride addition to TiO_2 at pH 3, shift the dominant surface species from $\equiv Ti–OH_2^+$ and $\equiv Ti–OH$ to $\equiv Ti–F$. By XPS analyzes it was also possible to corroborate the presence of $\equiv Ti–F$ species on TiO_2 surface in the fluorinated samples.

On the other hand, in Pt–S–TiO_2 sample the corresponding IR bands have significant lower intensities; this may be attributed to the high number of Pt particles on S–TiO_2 surface, as it was observed by TEM (Fig. 2A).

3.2. Phenol photodegradation

The evaluation of the photocatalytic activity of the materials prepared in this work was carried out by following the phenol photodegradation as test reaction.

TOC measurements after 120 min of reaction were carried out, practically total mineralization of phenol was reached for the fluorinated samples, i.e., 0.10 and 0.73 mg/L for F–TiO_2 and Pt–F–TiO_2 photocatalysts, respectively. The highest TOC value was obtained on bare TiO_2. According to HPLC analysis this remaining TOC was due to phenol and the intermediates catechol and hydroquinone.

Initial reaction rates in the phenol photodegradation over the analyzed photocatalysts are plotted in Fig. 7. As it can be seen in this figure, the photocatalytic activity of these materials greatly depends on TiO_2 modification.

The moderate activity of bare TiO_2 increased with Pt addition, it can be explained taking into account that Pt nanoparticles on TiO_2 surface act as a sink for the photogenerated electrons, thus retarding e^{-}–$h_{vb}{}^{+}$ pare recombination. It was also observed, a slight increase in phenol photodegradation rate after TiO_2 sulfation pretreatment. This increase can be due to the higher surface area and anatase stabilization obtained in the sulfated sample compared to the bare material. Besides, it has been reported [10,11] that in sulfated samples during the calcination a dehydroxylation process of the excess of adsorbed protons takes place, leading to the creation of surface oxygen vacancies, and promoting the separation of photogenerated charges, thus, improving the TiO_2 photocatalytic efficiency.

On the other hand, a high increase of the activity of the fluorinated sample (F-TiO_2) was observed, presenting an activity more than two fold the activity of bare TiO_2.

The enhancement of TiO_2 photoactivity for phenol degradation by fluorination or sulfation can be understood by a combination of different factors; firstly, an increase of the TiO_2 surface area was obtained after these treatments, leading to a better substrate adsorption during the photocatalytic reaction; F–TiO_2 sample presents a UV absorption higher than the other analyzed samples; in addition, fluorinated TiO_2 surface favors the generation of free •OH radicals creating oxygen vacancies and increasing the surface hydroxyl groups content [13,15], as it was observed by XPS analyzes. All these factors could contribute to an improvement of the TiO_2 activity.

It has also been reported that when the TiO_2 surface is covered by $\equiv Ti–F$ species, the photocatalytic degradation process is dominantly initiated by the direct transfer of the valence band holes, these conditions specifically favors the reaction of the photodegradation of phenol, this is mainly due to the direct electron transfer from the aromatic ring to the hole [13].

During the photocatalytic reaction, $\equiv Ti–F$ species could enhance the generation of free OH radicals by preventing the formation of $\equiv Ti–O^{\bullet}$ traps via direct oxidation of surface —OH groups Eq. (4). Valence band holes, $h_{vb}{}^{+}$, are not able to oxidize the F^{-} anion due to the too high oxidation potential of the $F^{\bullet}/F^{-}$ couple (3.6 V) [13]; thus, $h_{vb}{}^{+}$ directly react with water molecules at the interface, producing •OH radicals according to Eq. (5) [29]. Mobile (unbound) •OH radicals are stronger oxidants than the surface adsorbed •OH radicals and a higher concentration of •OH radicals can consequently accumulate in the presence of fluorinated titania and increase the photodegradation rate.

$$\equiv Ti - OH + h^{+}{}_{vb} \rightarrow \equiv Ti - O^{\bullet} + OH^{-} \quad (4)$$

$$\equiv Ti - F + h^{+}{}_{vb} + H_2O \rightarrow \equiv Ti - F + {}^{\bullet}OH + H^{+} \quad (5)$$

On the other hand, the surface $\equiv Ti–F$ groups can act as electron-trapping sites retaining photogenerated electrons due to the strong electronegativity of the fluoride. In this way, a more efficient charge separation will be produced, leading therefore to the enhancement of the TiO_2 photoefficiency [30].

XPS measurements have indicated the presence of surface OH groups and the formation of oxygen vacancies on TiO_2 surface due to the surface fluorination and/or sulfation. These modifications improve the photocatalytic activity in the phenol photodegradation under UV irradiation.

In the case of metallized samples, the addition of Pt to sulfated titania (Pt–S–TiO_2) notably increased the phenol photodegradation rate. As it was seen in TEM pictures (Fig. 2A), a homogenous distribution and a small metal particles size was attained in this sample. This would help platinum particles to act as electron traps improving the separation of the photogenerated charges in this sample.

On the other hand, platinization of fluorinated TiO_2, did not induce a significant change in the photoactivity of this material. In this case, Pt distribution on the surface was not very homogenous and particle sizes were larger (Fig. 2B) with the result that the effect of platinum is slightly noticed.

However, it is important to note that under the experimental conditions used in this work, the phenol photodegradation rate over Pt–S–TiO_2, is just a little higher than the rate obtained over F–TiO_2 sample. Taking into account the high cost of the noble metals, it appears that fluorination process is a good method to improve the efficiency of TiO_2 and could be an alternative to replace the metallization. However, as this effect will be much depending on

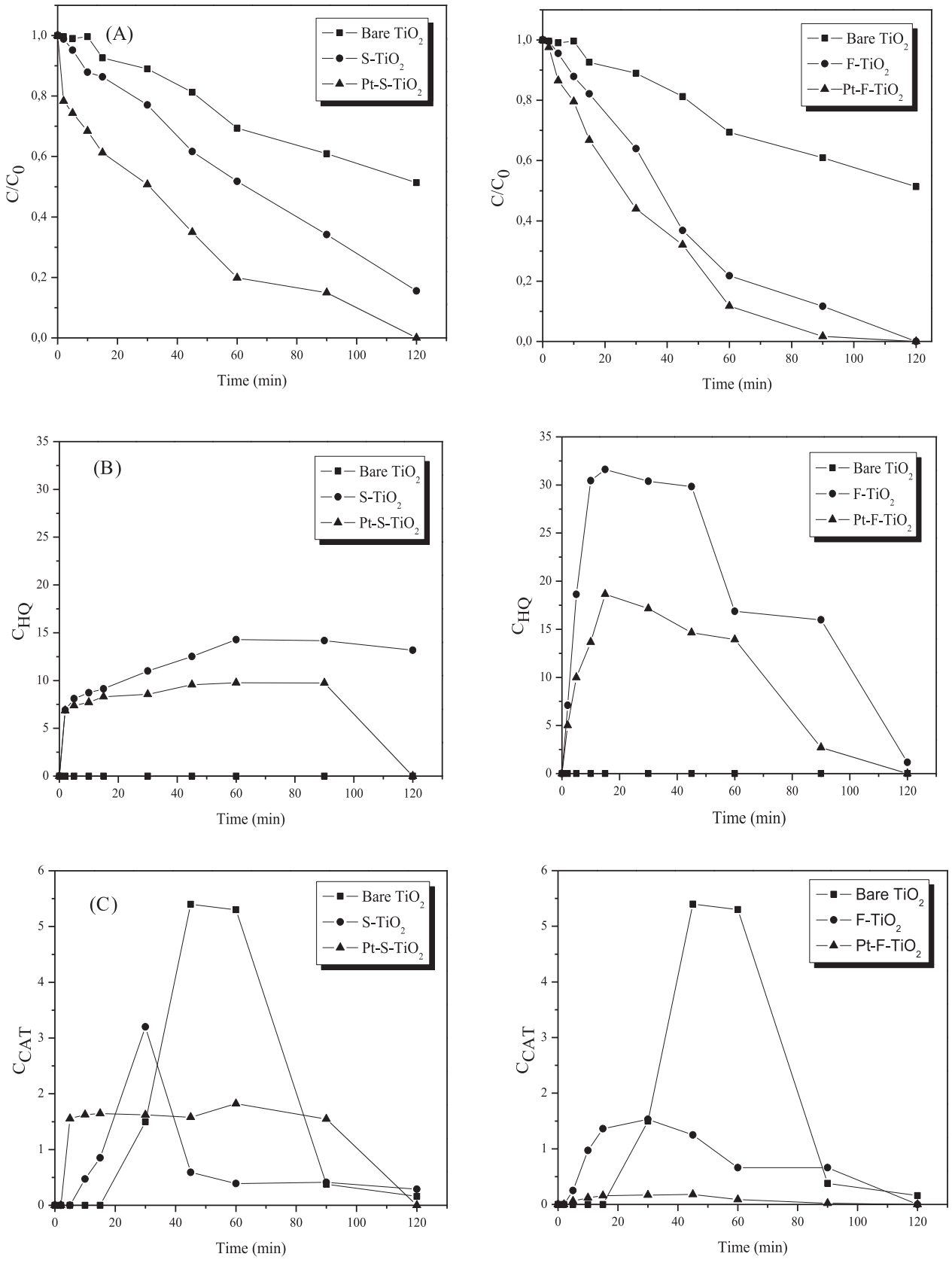

Fig. 6. Phenol and reaction intermediates concentration vs. irradiation time obtained with the different photocatalysts. (A) Phenol, (B) hydroquinone, and (C) cathecol.

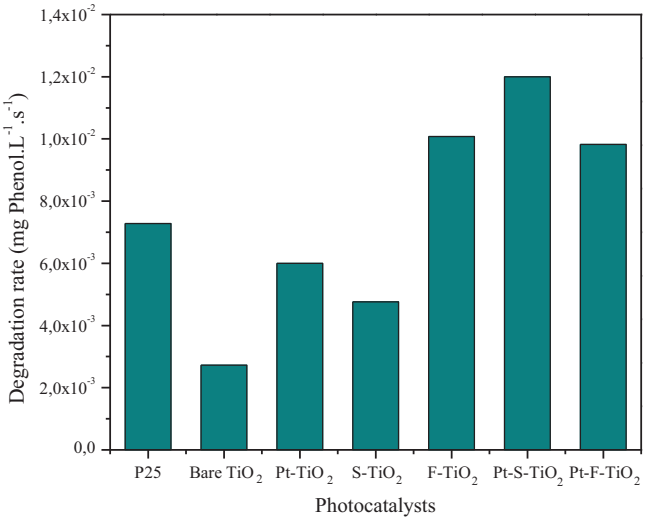

Fig. 7. Initial reaction rates for phenol photo-oxidation (milligram of phenol per litre and second) over analyzed photocatalysts.

the substrate to be degraded, studies in the degradation of other different organic pollutants will be interesting to follow.

By HPLC analysis catechol and hydroquinone were detected as the main intermediaries during the phenol photodegradation reaction. The evolution of the phenol and intermediaries species concentration as a function of photoreaction time using different photocatalysts is depicted in Fig. 6; as it can be observed the phenol concentration decreases with the reaction time (Fig. 6A).

No hydroquinone formation was observed on bare TiO_2 photocatalyst (Fig. 6A) but the highest catechol production was obtained on this sample (Fig. 6C). After sulfation or fluorination was evident the hydroquinone production, the highest content of this reaction intermediary was observed on F–TiO_2 sample. After platinization the intermediaries concentration decreases. In seems that chemical species on TiO_2 surface strongly modifies the adsorption and the substrate surface interactions, in fact, in a previous work we have demonstrated that on Pt–TiO_2 photocatalysts there are different adsorption centers in respect to bare TiO_2 and surface Pt atoms can also act as adsorption centers for phenol. Also the ions of Na, Cl, and S on surface can be involved in the photodegradation reaction mechanism.

It is possible that on F–TiO_2 catalyst the displacement of —OH by F— also changes the phenol adsorption as it has been reported by Minero et al. [13], this displacement may leads to the formation of •OH free radicals, which are more reactive than bounded •OH radicals. It is possible that the phenol photodegradation on F–TiO_2 photocatalyst takes place through the reaction with •OH radical leading to the faster degradation of phenol via formation of catechol and hydroquinone simultaneously.

4. Conclusions

Phenol photodegradation rate can be significantly improved by TiO_2 sulfation, fluorination and Pt photodeposition.

The highest photocatalytic activity was obtained on Pt–S–TiO_2 sample; due to a combined effect between an improved separation of photogenerated charges and a better Pt nanoparticles distribution on TiO_2 surface.

The phenol photodegradation rate over F–TiO_2 sample was very close to the rate obtained on Pt–S–TiO_2 sample. In the former sample, the beneficial effects of fluorination leading to a high hydroxylated surface and high surface, leading to a high degradation rate, avoiding the need of expensive noble metal deposition to reach the same degree of activity. This appeared as a promising alternative for TiO_2 modification.

Acknowledgements

This research was financed by the Spanish Ministerio de Ciencia e Innovación (Project Ref. CTQ2011-26617-C03-02). J.J. Murcia would like to thank CSIC for the concession of a JAE grant. CITIUS (University of Seville) is acknowledged for XPS and XRF measurements.

References

[1] S.G. Kumar, L.G. Devi, J. Phys. Chem. A 115 (2011) 13211–13241.
[2] M. Qamar, Int. J. Nanosci. 9 (2010) 579–583.
[3] A. Fujishima, X. Zhang, D.A. Tryk, Surf. Sci. Rep. 63 (2008) 515–582.
[4] A.A. Ismail, D.W. Bahnemann, J. Phys. Chem. C 115 (2011) 5784–5791.
[5] M.C. Hidalgo, J.J. Murcia, J.A. Navío, G. Colón, Appl. Catal. B 397 (2011) 112–120.
[6] J.J. Murcia, J.A. Navío, M.C. Hidalgo, Appl. Catal. B 126 (2012) 76–85.
[7] J.J. Murcia, M.C. Hidalgo, J.A. Navío, J. Araña, J.M. Doña-Rodríguez, Appl. Catal. B 150–151 (2014) 107–115.
[8] A.V. Vorontsov, E.N. Savinova, J. Zhensheng, J. Photochem. Photobiol. A 125 (1999) 113–117.
[9] S.S. Srinivasan, J. Wade, E.K. Stefanakos, Y. Goswami, J. Alloys Compd. 424 (2006) 322–326.
[10] M.C. Hidalgo, M. Maicu, J.A. Navío, G. Colón, Appl. Catal. B. 81 (1–2) (2008) 49–55.
[11] G. Colón, M.C. Hidalgo, J.A. Navío, Appl. Catal. B 45 (2003) 39–50.
[12] M.V. Dozzi, E. Selli, Catalysts 3 (2013) 455–485.
[13] C. Minero, G. Mariella, V. Maurino, E. Pelizzetti, Langmuir 16 (2000) 2632–2641.
[14] M.S. Vohra, S. Kim, W. Choi, J. Photochem. Photobiol. A 160 (2003) 55–60.
[15] T.K. Le, D. Flahaut, H. Martinez, T. Pigot, H.K.H. Nguyen, T.K.X. Huynha, Appl. Catal. B 144 (2014) 1–11.
[16] S. Liu, J. Yu, B. Cheng, M. Jaroniec, Adv. Colloid Interface Sci. 173 (2012) 35–53.
[17] J. Kim, J. Lee, W. Choi, Chem. Commun. (2008) 756–758.
[18] H. Park, W. Choi, J. Phys. Chem. B 108 (2004) 4086–4093.
[19] J. Yu, W. Wang, B. Cheng, B.L. Su, J. Phys. Chem. C 113 (2009) 6743–6750.
[20] H. Park, Y. Park, W. Kim, W. Choi, J. Photochem. Photobiol. C 15 (2013) 1–20.
[21] D. Hufschmidt, D. Bahnemann, J.J. Testa, C.A. Emilio, M.I. Litter, J. Photochem. Photobiol. A 148 (2002) 223–231.
[22] D. Li, H. Haneda, S. Hishita, N. Ohashi, N.K. Labhsetwar, J. Fluorine Chem. 126 (2005) 69–77.
[23] K. Okazaki, Y. Morikawa, S. Tanaka, K. Tanaka, M. Kohyama, J. Mater. Sci. 40 (2005) 3075–3080.
[24] J. Yu, Q. Xiang, J. Rana, S. Mann, Cryst. Eng. Commun. 12 (2010) 872–879.
[25] S. Yamabi, H. Imai, Chem. Mater. 14 (2002) 609–614.
[26] J. Araña, J.M. Doña-Rodríguez, O. González-Díaz, E. Tello Rendón, J.A. Herrera Melián, G. Colón, J.A. Navío, J. Pérez Peña, J. Mol. Catal. A: Chem. 215 (2004) 153–160.
[27] P.A. Connor, K.D. Dobson, A.J. McQuillan, Langmuir 15 (1999) 2402–2408.
[28] M. Takeuchi, G. Martra, S. Coluccia, M. Anpo, J. Phys. Chem. C 111 (2007) 9811–9817.
[29] M. Mrowetz, E. Selli, Phys. Chem. Chem. Phys. 7 (2005) 1100–1102.
[30] J.C. Yu, J. Yu, W. Ho, Z. Jiang, L. Zhang, Chem. Mater. 14 (2002) 3808–3816.